11-2014

Direct Numerical Simulations of Non-premixed ethylene–Air Flames: Local Flame Extinction Criterion

Vivien R. Lecoustre

Paul G. Grias

Somesh P. Roy

Zhaoyu Luo

Dan C. Haworth

See next page for additional authors

Authors

Vivien R. Lecoustre, Paul G. Grias, Somesh P. Roy, Zhaoyu Luo, Dan C. Haworth, Hong G. Im, Tianfeng F. Lui, and Arnaud Trouvé

Combustion and Flame, Vol. 161, No. 11 (November 2014) : 2933-2950. DOI.

Direct Numerical Simulations of Non-premixed ethylene–Air Flames: Local Flame Extinction Criterion

Vivien R. Lecoustre
Fire Protection Engineering, University of Maryland, College Park, MD
Paul G. Arias
Clean Combustion Research Center, King Abdullah University of Science and Technology, Thuwal 23955, Saudi Arabia
Department of Mechanical Engineering, University of Michigan, Ann Arbor, MI
Somesh P. Roy
Department of Mechanical and Nuclear Engineering, Pennsylvania State University, University Park, PA
Zhaoyu Luo
Department of Mechanical Engineering, University of Connecticut, Storrs, CT
Dan C. Haworth
Department of Mechanical and Nuclear Engineering, Pennsylvania State University, University Park, PA
Hong G. Im
Clean Combustion Research Center, King Abdullah University of Science and Technology, Thuwal 23955, Saudi Arabia
Department of Mechanical Engineering, University of Michigan, Ann Arbor, MI

Tianfeng F. Lue
Department of Mechanical Engineering, University of Connecticut, Storrs, CT
Arnaud Trouvé
Fire Protection Engineering, University of Maryland, College Park, MD

Abstract

Direct Numerical Simulations (DNS) of ethylene/air diffusion flameextinctions in decaying two-dimensional turbulence were performed. A Damköhler-number-based flame extinction criterion as provided by classical large activation energy asymptotic (AEA) theory is assessed for its validity in predicting flame extinction and compared to one based on Chemical Explosive Mode Analysis (CEMA) of the detailed chemistry. The DNS code solves compressible flow conservation equations using high order finite difference and explicit time integration schemes. The ethylene/air chemistry is simulated with a reduced mechanism that is generated based on the directed relation graph (DRG) based methods along with stiffness removal. The numerical configuration is an ethylene fuel strip embedded in ambient air and exposed to a prescribed decaying turbulent flow field. The emphasis of this study is on the several flame extinction events observed in contrived parametric simulations. A modified viscosity and changing pressure (MVCP) scheme was adopted in order to artificially manipulate the probability of flame extinction. Using MVCP, pressure was changed from the baseline case of 1 atm to 0.1 and 10 atm. In the high pressure MVCP case, the simulated flame is extinction-free, whereas in the low pressure MVCP case, the simulated flame features frequent extinction events and is close to global extinction. Results show that, despite its relative simplicity and provided that the global flame activation temperature is correctly calibrated, the AEA-based flame extinction criterion can accurately predict the simulated flame extinction events. It is also found that the AEA-based criterion provides predictions of flame extinction that are consistent with those provided by a CEMA-based criterion. This study supports the validity of a simple Damköhler-number-based criterion to predict flame extinction in engineering-level CFD models.

Keywords

Flame extinction, Turbulent diffusion flame, , Direct numerical simulation, Chemical Explosive Mode Analysis, Extinction criterion

1. Introduction

Flame extinction in non-premixed flames is a central subject of research in combustion science that has important ramifications for engineering applications; whether the interest lies in power generation applications or in fire safety. The seminal work of Liñán [1] has provided the mathematical foundations for the study of non-premixed flame extinction in laminar counter-flow configurations. Several authors have since then extended the extinction analysis to different non-premixed flame configurations [2], [3], [4], with various level of heat losses [4], [5], and turbulent conditions [6]. Further references and descriptions are provided in the reviews by Williams [7], [8]. These studies have shown that extinction can be explained by the concept of a critical value of a Damköhler number, defined as the ratio of a characteristic mixing time divided by a characteristic chemical time.

Direct Numerical Simulations (DNS) provide a valuable platform for the understanding of the physics of flames. Several past DNS works and analysis using DNS data have focused on non-premixed flame extinction in various environments [9], [10], [11], [12], [13], [14], [15], [16], [17]. Dependence of local extinction and reignition on the overall mixing in CO/H_2 non-premixed turbulent jet flames were studied using the one-dimensional turbulence model by Hewson and Kerstein [9]. It was shown that the actual probability of

extinguished fluid (taken as local condition with temperature lower than 1000 K) is greater than the probability that the critical extinction scalar dissipation rate, obtained from laminar steady-state flamelet consideration, is exceeded. It was also concluded that the rate of reignition scales with the global mixing rate, as the mixing increases the rate of heat transfer between stoichiometric regions. An extension of the flamelet model was proposed by Pitsch et al. [10] to account for flame reignition, and compared with DNS data. The updated model includes the transport terms along the stoichiometric iso-surface – which are usually neglected in the flamelet approach – to account for the heat exchange between flamelets. The model assumed reignition by edge-flame propagation along the stoichiometric iso-surface. Analysis on the *S* curve show that the addition of these extra terms allows to predict flame reignition with satisfactory agreements with DNS data.

Sripakagorn et al. [11] performed DNS of 3D, non-premixed flame immersed in an isotropic, decaying turbulent field to study the mechanisms of flame extinction and reignition. Single step chemistry and Lagrangian flame element tracking technique were employed to examine the dynamics response of chosen flame elements with turbulence. The observed extinction events were attributed to be principally caused by excessive heat losses for local scalar dissipation rate exceeding values of extinction of steady state flames. Extinguished flame elements were identified as those with stoichiometric temperature lower than that possible for a steady-state flamelet at elevated scalar dissipation rate. Their results show that while the 1D flamelet model predicts extinction very well, it does not predict most of the re-ignition events. Three different flame reignition scenarios were identified, each involves different levels of neighboring flame interaction. The independent flamelet scenario does not involve any interaction with the neighboring flame elements, while edge flame propagation and engulfment scenarios involve strong interactions with the neighboring, either through important lateral positive diffusion of heat from a hot neighboring stoichiometric region toward the cold region, or heat transport to the cold region via turbulence motion, respectively.

Two dimensional DNS investigations of extinction and re-ignition were performed by Venugopal and Abraham [13]. Their numerical configuration was that of a n-heptane laminar non-premixed flame at 40 bar interacting with counter-rotating vortex pairs. Effects of unsteadiness and curvature on flame extinction and reignition were explored. Using an irreversible single-step reaction model, they show that extinction are well captured with 1D transient diffusion flamelet libraries that account for the time history of the scalar dissipation rate, while reignition involves flame-flame interactions and is affected by the local flame topology. A local Damköhler number was defined and extinction was identify when the Damköhler number reached 1. Analysis of the extinction mechanisms has shown that the heat losses by convection along the direction normal to the stoichiometric iso-surface is the dominant mode of heat losses followed by the diffusive heat losses along this direction. Further analysis show that while extinction is a 1D phenomenon, the curvature has a significant effect on the rate of increase of the stoichiometric scalar dissipation rate.

Lignell et al. [14] performed a parametric study of flame extinction and reignition in non-premixed ethylene/air flames using a 3D DNS configuration with detailed chemistry similar to that of Hawkes et al. [12]. Varying Damköhler number at fixed Reynolds was considered. They predicted that flames with increased level of extinction have increased stoichiometric scalar dissipation rate and have shown that the probability density function of the stoichiometric scalar dissipation rate is very close to that of a lognormal distribution, with however some deviation from it at low and high scalar dissipation rate. A positive correlation between scalar dissipation rates and flame curvature was exhibited, with extinction occurring preferentially in flame region with the center of curvature being located in the fuel stream. Mechanisms for flame reignition were identified and were very similar to that of [11], with the addition of flame reignition mechanism due to premixed flames propagation. In contrast to the work of Sripakagorn, access to detailed flame structure allows to distinguish between edge-flame propagation and premixed flames.

Past work by our group was focused on flame extinction diagnostics in different flame extinction configurations: by convective cooling due to flame interactions with a cold wall [15], by thermal radiation losses due to high soot loading [16], by evaporative cooling due to water-spray [17]. Narayanan et al. [18], have studied a Damköhler-number-based flame extinction criterion using large activation energy asymptotic (AEA) analysis and explored the extinction limits of laminar counter-flow diffusion flames as a function of flame stretch and radiant losses due to soot and gas-phase species. A parametrization of this Damköhler number criterion was performed in subsequent work for diffusion flame conditions with various levels of stretch, radiation losses, and air or fuel vitiation [19]. These studies confirm the early concept of a critical value of a Damköhler number for flame extinction; note, however, that they are limited to a global single-step representation of the combustion chemistry.

The objectives of this present work are to perform DNS of non-premixed flame extinction resulting from sustained high mixing intensities, and to study the applicability of the AEA-based critical Damköhler number flame extinction criterion to turbulent-like flames described with detailed chemistry.

Different cases are simulated in order to achieve different combustion regimes: from extinction-free flames under high Damköhler number conditions to flames with frequent extinction events under low Damköhler number conditions. Changes in Damköhler number conditions are implemented using a modified viscosity and changing pressure (MVCP) scheme: the MVCP scheme allows simulating cases with identical flow conditions and flames that are weakened or strengthened at will. The simulated flames are first analyzed using the classical AEA-based flame Damköhler number. Next, they are analyzed using a more elaborate flame Damköhler number provided by a Chemical Explosive Mode Analysis (CEMA) [20]. The comparison between DNS, AEA, and CEMA provides an evaluation of our ability to predict diffusion flame extinction under turbulent flow conditions.

2. Numerical methods

2.1. Navier–Stokes solver

The DNS solver employs an explicit 4th order Runge–Kutta (ERK) time integration scheme [21] and an 8th order central finite-differencing scheme [22] for accurate integration of the compressible form of the Navier–Stokes equations. Spatial filtering is performed using a purely-dissipative 10th order filter [22]. Boundary conditions are treated using Navier–Stokes Characteristic Boundary Conditions (NSCBCs) described in Ref. [23]. Further information and discussion on the governing equations and the boundary conditions can be found in Refs. [15], [24], [17], [14] and references therein.

Transport properties are evaluated using a mixture averaged model, calculated from the transport libraries provided by wrappers to the CHEMKIN package [25]. The code is highly modular, incorporating advanced multi-physics such as radiation [15], soot models [16], water droplet dynamics [17], that have previously been used.

2.2. Reduced chemical model

The detailed mechanism used was first proposed by Appel et al. [26]. It is a C_2H_4-air combustion model featuring 101 species and 542 elementary reactions. It includes growth of polycyclic aromatic hydrocarbons (PAH) beyond benzene through the HACA mechanism up to pyrene ($C_{16}H_{10}$). The detailed mechanism is too large in size and presents strong stiffness that precludes its use for DNS applications. The integrated approach presented in Ref. [27] was employed to reduce the mechanism and remove any chemical stiffness, rendering it suitable to DNS application. It is noted that the reduced mechanism with PAH chemistry was first developed for DNS of sooting flames [28], [29], [30].

First, the method of DRG-aided sensitivity analysis was applied to eliminate unimportant species and reactions from the detailed mechanism. A skeletal mechanism with 67 species and 342 reactions was obtained that

provided relatively accurate predictions (within 20% of those provided by the detailed mechanism) in ignition delays, extinction times in perfectly stirred reactors (PSR), pyrene concentrations in PSR, and laminar premixed flame speeds.

The domain of validity of the skeletal mechanism covered pressures between 0.1 and 10 atm, equivalence ratios between 0.5 and 2.0, and initial temperatures above 1000 K for ignition. Linearized quasi steady state approximations (LQSSA) were subsequently applied to seven species, namely CH, CH_2, CH_2•, CH_2OH, CH_3O, C_2H, *n*-C_6H_5, which were identified to be in quasi steady state (QSS) for all the investigated conditions using a criterion based on computational singular perturbation [27].

A 56 step reduced mechanism was then obtained with the QSS species concentrations solved analytically [31]. Finally, dynamical stiffness removal [27] was applied on the mechanism to eliminate chemical time scales shorter than 10 ns. This cutoff time step value is comparable to the limit imposed by the Courant–Friedrichs–Lewy (CFL) condition in our compressible flow simulations, where a typical time step Δt = 7 ns is adopted. The final reduced mechanism contains 60 species.

Figure 1 shows the validation of the skeletal and the reduced mechanisms compared with the detailed (original) model for auto-ignition (Fig. 1a), extinction PSR (Fig. 1b), in a 1D counter flow non-premixed flame with ethylene (Fig. 1c), and 1D laminar premixed flames (Fig. 1d), respectively.

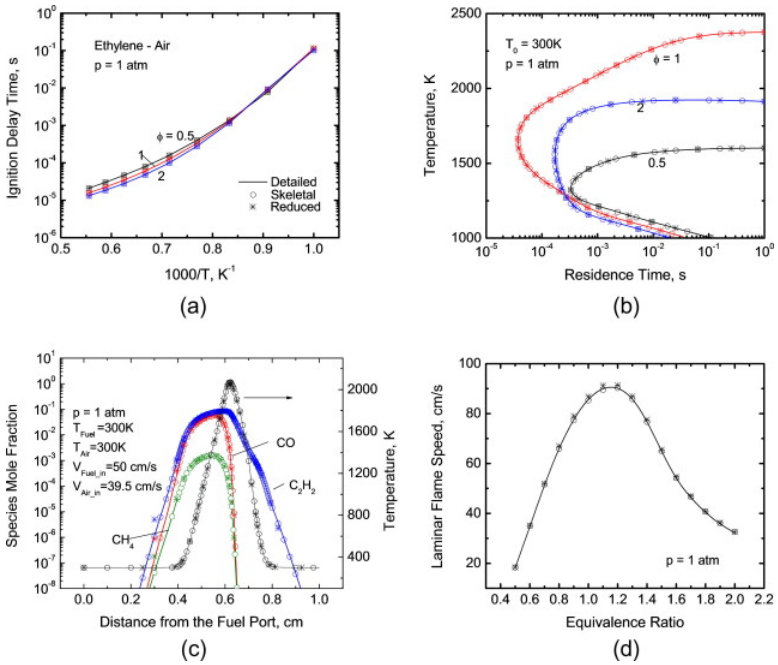

Fig. 1. Comparison of the 67-species skeletal mechanism and 60-species reduced mechanism with the detailed mechanism for (a) ignition delay, (b) extinction temperature profiles in PSR, (c) temperature and species profiles in a counter flow non-premixed flame with ethylene (x = 0) and air (x = 1 cm), and (d) 1D laminar premixed flame speed for stoichiometric ethylene–air at STP.

2.3. Problem configuration

Our goal is to numerically simulate diffusion flame extinction and to evaluate the AEA-based Damköhler number flame extinction criterion. Since the dynamics of the turbulence are not of interest but only their stirring and flame wrinkling effects, a 2D configuration is adopted a cost-effective framework for the present investigation. While the flame-flow interactions are different in 2D and 3D, the present 2D approach is justified by the assumption that the extinction dynamics are controlled by the same time-scale-ratio argument and described by the same Damköhler number criterion. Moreover, past findings by Sripakagorn et al. [11], and

Venugopal and Abraham [13] indicate that flame extinction, in contrast with flame reignition, is inherently a 1D phenomenon.

For the three pressure cases considered, the numerical configuration is that of a temporally evolving diffusion flame initially immersed in a decaying turbulent field. Each flame initial condition corresponds to that of a 1D laminar diffusion flame with an imposed moderate stoichiometric scalar dissipation rate of about 7s-1±20%. The fuel stream is pure ethylene and the oxidizer stream is air. The stoichiometric scalar dissipation rate, denoted χst, is defined as:

$$(1)\ \chi_{st} = 2\alpha_{mixture} \parallel \nabla Z \parallel^2_{Z=Z_{st}} ,$$

where Z is the mixture fraction, calculated using Bilger's formula presented in Ref. [32], αmixture is the mixture local thermal diffusivity, the subscript st denotes conditions at stoichiometry. This value is far from χ_{st} at extinction predicted by laminar counterflow flame simulations at 1 and 10 atm, which are 95.5 and 465 s-1, respectively. But it is close to extinction at 0.1 atm: predicted value is 12.5 s^{-1}. See Table 1.

Table 1. Stoichiometric scalar dissipation rate and temperature predicted at extinction conditions for the pressures considered. The corresponding activation temperature, Ta, is also tabulated. Ta has been calculated from the values of the laminar flame speed of simulated premixed flames at the pressures considered with the modified viscosity approach.

P (atm)	χq,ref (s^{-1})	Tq,ref (K)	T_a (K)
0.1	12.5	1475	12,292
1	95.5	1591	18,692
10	465	1780	19,250

The initial temperature and species fields were initialized by first mapping the physical space with a 1D mixture fraction profile. This profile of mixture fraction was generated with the following expression:

$$(2)\ Z(x) = \frac{1}{2}\left[erf\left(\frac{\frac{b}{2}+x}{\sqrt{2\sigma^2}}\right) + erf\left(\frac{\frac{b}{2}-x}{\sqrt{2\sigma^2}}\right)\right].$$

This expression corresponds to the exact solution of the problem of a fuel strip of width b diffusing in a quiescent environment. The slope of the mixture fraction profile at the stoichiometric point was adjusted by choosing the parameters σ and b such that the scalar dissipation rate takes the desired value. The width of the fuel strip, defined as the initial distance between the two stoichiometric points $Z_{st} = 0.064$, was 0.8 cm. As a result of these modeling choice, the peak mixture fraction value was 0.75 and not 1. However, this bears little importance in this work's conclusions. Figure 2 plots this mixture fraction profile.

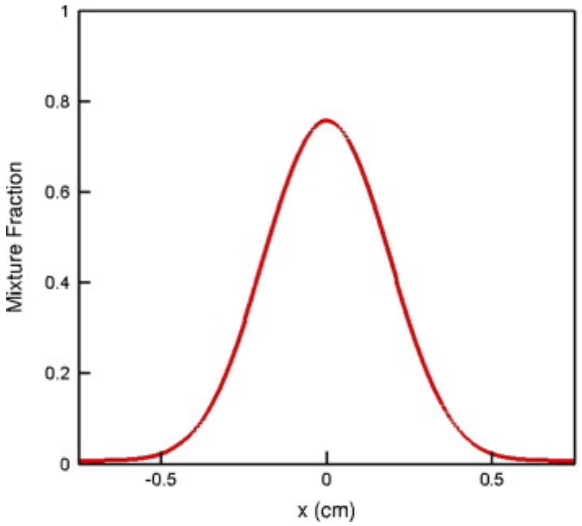

Fig. 2. Initial mixture fraction profile along the *x* axis. The total *x*-domain length is 2.4 cm. The slope of the profile was adjusted so that at location of stoichiometry, the value of the scalar dissipation rate is χ_{st} = 7 s^{-1}.

Temperature and species fields were initialized using a flamelet solution generated in a counter-flow configuration with a matching value of χ_{st}. The flamelet was generated with OPPDIF [33] using the same chemical kinetics mechanism. The initial flame profile was immersed into an isotropic, homogeneous 2D turbulent flow field generated with the Passot–Pouquet energy spectrum [34]:

$$(3)\quad E(k) = \frac{32}{3}\sqrt{\frac{2}{\pi}}\frac{u'^2}{k_e}\left(\frac{k}{k_e}\right)^4 \exp\left[-2\left(\frac{k}{k_e}\right)^2\right].$$

The RMS fluctuating velocity, u', was set to 8 m/s while the mean velocity was set to 0. The size of the most energetic eddies was set to 1 mm. The integral length scale and the Kolmogorov length scale were equal to 0.34 mm and 14 µm, respectively. The eddy turn-over time was 40 µs and the initial turbulent Reynolds number, ReT, was equal to 173.

The same turbulent parameters were used for all cases. In order to minimize the interactions between the turbulent flow and the boundaries of the computational domain, the turbulent field was spatially filtered within 5 mm near each $\vec{x}$ boundary at initialization. This limited any artificial pressure disturbance that may occur when a vortex leaves the computational domain during the time of the computation.

The rectangular, two-dimensional computational domain was 2.4 cm long in the $\vec{x}$ direction and 1.4 cm wide in the $\vec{y}$ direction. A uniform, Cartesian mesh was used with a grid spacing of 8 µm. This value represents the minimum grid resolution required to accurately resolve the flames structure near strain-induced extinction for all the pressures considered in the present study (see Fig. 3, Fig. 4). This value was determined using OPPDIF, by simulating a steady-state counter-flow diffusion flame near strain-induced extinction conditions and using the modified viscosity and species diffusivity approach described in Section 2.4. Species reaction profiles were investigated for various grid spacings. The grid spacing was chosen so that the distance between successive peaks in the reactions rate profiles was resolved by approximately 10 equally-spaced points. Fig. 3, Fig. 4 show the reaction rate profiles of selected species at 10 atm as the representative results for grid resolution study. The desired level of resolution is achieved only for grid spacing values less than 10 µm. Similar tests were performed at 0.1 atm and 1 atm and 8 µm grid spacing was found to be sufficient.

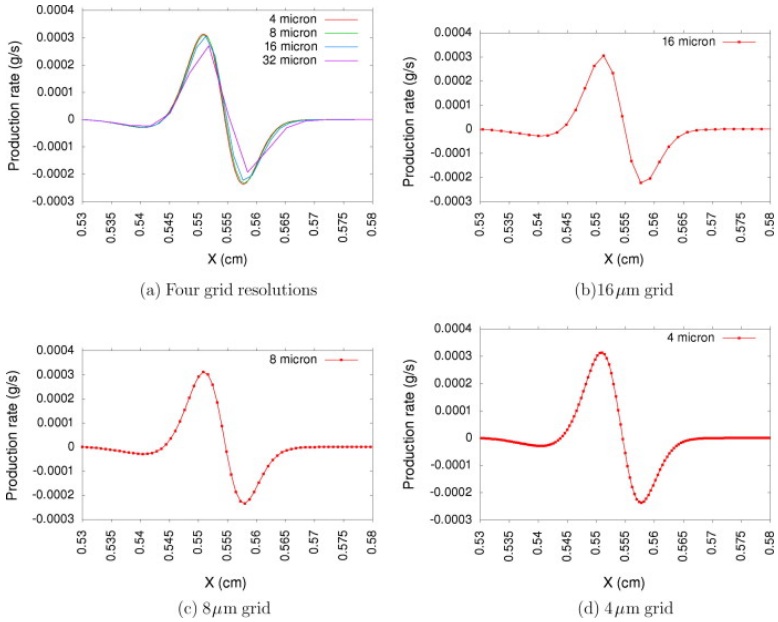

(a) Four grid resolutions

(b)16 μm grid

(c) 8 μm grid

(d) 4 μm grid

Fig. 3. Profiles of reaction rate of HCCO for a counter-flow diffusion flamenear strain-induced extinction conditions simulated with OPPDIF using uniform meshes with different grid spacing. Modifications of transport coefficients as describes in Section 2.4 was employed. Grid spacings considered: 32, 16, 8, and 4 µm. Pressure is 10 atm. The distance between the two peaks in the reaction rate is approximately 100 µm.

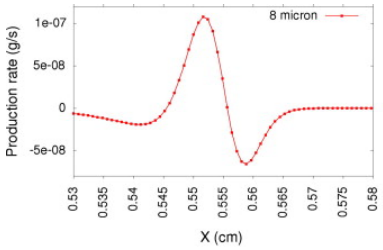

(a) Production rate of CH_3O, grid spacing of 8 μm

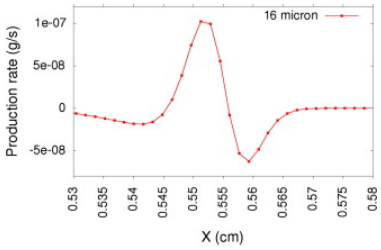

(b) Production rate of CH_3O, grid spacing of 16 μm

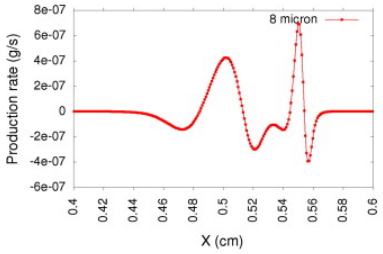

(c) Production rate of $n-C_4H_5$, grid spacing of 8 μm

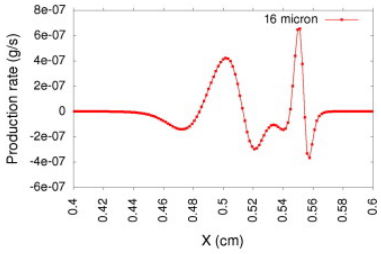

(d) Production rate of $n-C_4H_5$, grid spacing of 16 μm

Fig. 4. Profiles of reaction rate of CH_3O and C_4H_5 for a counter-flowdiffusion flame near strain-induced extinction conditions simulated with OPPDIF using uniform meshes with different grid spacing. Modifications of transport coefficients as describes in Section 2.4 was employed. Grid spacings considered: 16 and 8 µm. Pressure is 10 atm. The minimum distance between peaks in the reaction rate profiles is approximately 100 µm.

The total number of grid point was 5,250,000: 3000 points in the *x*-direction, 1750 points in the *y*-direction. The workload was shared by 2100 cores using the National Energy Research Scientific Computingcenter (NERSC) Cray XE6 “Hopper” and the now-retired Cray XT4 “Franklin”. The time step was chosen depending on the pressure and based on CFL considerations. At *P* = 0.1 atm, the time step was set to 10 ns; at atmospheric pressure, it was

set to 7.2 ns; and at *P* = 10 atm, the time step was set to 5 ns. Each simulation represents about 200,000 CPU hours.

2.4. The modified viscosity and changing pressure (MVCP) scheme

The pressure was manipulated in order to achieve different combustion regimes: higher pressures strengthen the flame and decrease the occurrence of flame extinction, while lower pressures weaken the flame and increase the occurrence of flame extinction. Thus, changing pressure provides a simple control on the combustion strength and thereby allows testing the AEA-based flame extinction criterion. The same configuration was considered at 0.1, 1, and 10 atm. As the focus of this work is the chemical kinetic response of the flame under aerodynamic strain, it is desired to keep the turbulence characteristics (turbulent Reynolds number, turbulent kinetic energy, integral length scale, eddy turn-over time, Kolmogorov length scale) independent of pressure. Turbulent flow characteristics at 1 atm were established as reference.

The Kolmogorov theory states that the dynamics of the turbulence are controlled by the large scales and by the kinematic viscosity ν. If the large scales properties are kept identical for all cases, then in order to obtain the same turbulent flow dynamics, ν must be kept independent of pressure. Now $\nu = \frac{\mu}{\rho}$, where ρ is the mass density of the fluid, and consideration of the ideal gas law gives:

$$(4) \quad \nu \sim \frac{1}{P}.$$

In order to keep the kinematic viscosity independent of pressure, the dynamic viscosity μ of the fluid has to vary linearly with pressure:

$$(5) \quad \mu = \mu_0 P.$$

This allows identical turbulent evolution when the same initial conditions are applied to the system regardless of the pressure considered.

All molecular transport properties were scaled accordingly and the mixture conductivity and the species diffusivity were adjusted so that the Prandtl, Lewis, and Schmidt numbers were unaffected by the modification of the dynamic viscosity. This provides a unique and consistent configuration for which only the chemical source terms were affected by changes in pressure but not the flow field. In conclusion, we use in the present study a modified viscosity and changing pressure (MVCP) scheme that provides convenient but artificial control on the flame-flow coupling and the Damköhler number conditions. It is worth emphasizing that while the MVCP scheme uses changes in pressure, it also uses a modified viscosity model and the DNS simulations are therefore not representative of real pressure effects.

3. Results

3.1. Verification of MVCP scheme

The present MVCP scheme has been verified by comparing the flame shape and the statistical distribution of the scalar dissipation ratebetween the different pressure cases. This comparison was performed in simulations using the detailed chemistry model presented in Section 2.2as well as in simulations using a single step chemistry model adopted in earlier work [15]. The computationally cheaper single-step chemistry was first used in lieu of the detailed chemistry in order to verify that the turbulent flow field kept the same characteristics (i.e. turbulent Reynolds number, turbulent kinetic energy, integral length scale, eddy turn-over time, Kolmogorov length scale) regardless of the pressure.

For the sake of illustration, the temperature fields obtained with this single step chemistry model at 0.5 ms at 1 and 10 atm are presented in Fig. 5. Figure 6 plots the corresponding scalar dissipation rate χ at $Z = Z_{st}$ at 0.5 ms. The distributions are nearly identical. The mean, maximum, minimum values, and standard deviation of the scalar dissipation rate are similar for these two pressures; at *P* = 1 atm, the mean χst is 26.4 s^{-1} and the standard deviation is 34.7 s^{-1}; at *P* = 10 atm, the mean χst is 26.7 s^{-1} and the standard deviation is 32.6 s^{-1}. Some small differences are nevertheless observed. These are mostly due to the slight changes in temperature observed with different pressure, which lead to slight modification of the viscosity and diffusivity and thereby modify the gradients.

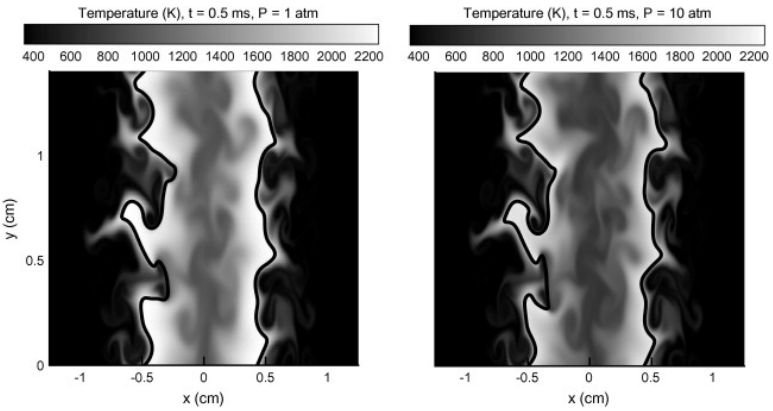

Fig. 5. Instantaneous temperature fields at 0.5 ms at cases at 1 atm and 10 atm. For the case at 10 atm, the viscosity was modified to keep the turbulence identical to that in the 1 atm case. A single step chemistry model was used here to simulate both flames. The solid black line indicates the flame stoichiometric isocontour.

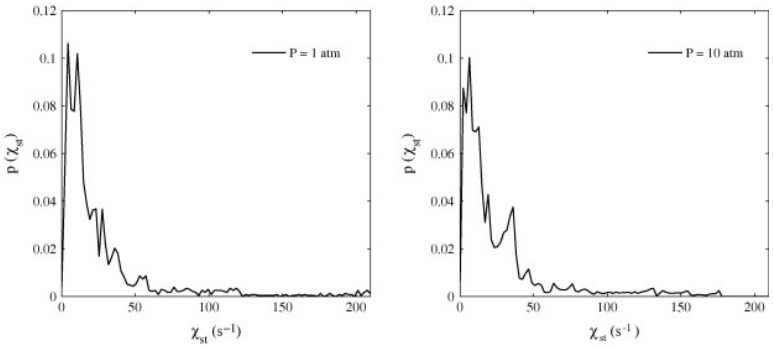

Fig. 6. Probability density distribution of instantaneous stoichiometric scalar dissipation rates χst predicted at 1 atm (left) and 10 atm (right), 0.5 ms after initialization. A single step chemistry model was used here for both simulations.

The effects of modified viscosity on flame chemistry were investigated by simulating a laminar pure ethylene/air counterflow diffusion flamewith OPPDIF at 10 atm. Figure 7 compares the predicted temperature spatial profiles and the flamelet profiles of temperature, radical H, radical OH, CO, and CO_2 with and without the modified viscosity approach, respectively. The stoichiometric scalar dissipation rate was kept constant. Effects of change in viscosity (and species diffusivity in order to keep the Lewis, Schmidt numbers invariant under this transformation) show that as expected: the profile of temperature is broadened with changed of viscosity at high pressure, while the species profiles are invariant with this change.

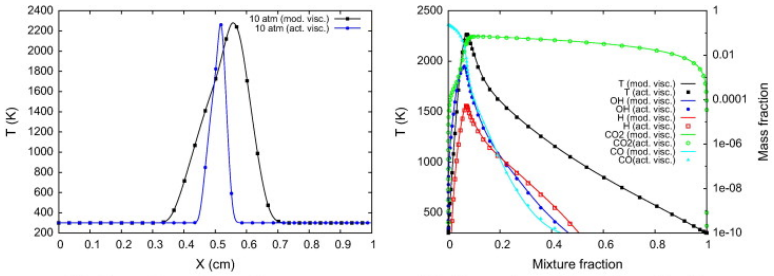

(a) Comparison of spatial temperature profile with and without modified viscosity at 10 atm.

(b) Comparison of flamelet profile of selected species and temperature with and without modified viscosity at 10 atm.

Fig. 7. Predicted temperature profiles and flamelet profiles in an ethylene–air counterflow diffusion flame with OPPDIF at 10 atm. Comparison between solutions predicted with and without the modified viscosity is shown.

Figure 8 presents another verification test. The temporal evolution of the volume integrated turbulent kinetic energy is plotted for the three pressures considered using the reduced multi-species chemical model. All the simulations start with the same level of turbulent kinetic energy in the domain. This plot shows that the initial decay of the turbulent kinetic energy is similar in all the cases. Some differences arise in the later stages of the simulations due to the different flame responses to the aerodynamic strain: some extinction and re-ignition events are observed at lower pressure, but none at high pressure; and due to the differences in flame temperature: peak flame temperature increases with pressure.

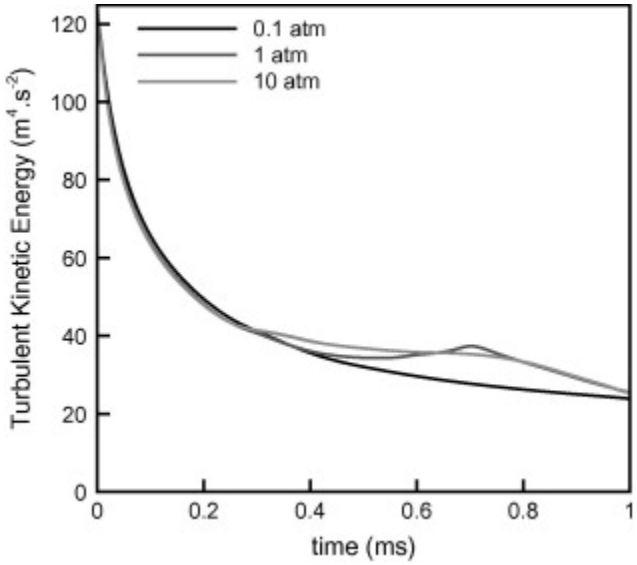

Fig. 8. Temporal evolution of the volume-integrated turbulent kinetic energy (TKE), ∫D12u′2+v′2dxdy in simulations at 0.1, 1, and 10 atm.

3.2. Flame evolution

Fig. 9, Fig. 10, Fig. 11 plot the instantaneous temperature field at various times in the simulations, from initialization to the end of the simulation, set at 1 ms. The pressure in Fig. 9 is 1 atm, whereas it is 10 atm in Fig. 10, and 0.1 atm in Fig. 11. As a result of the modified viscosity approach, the temporal evolution of the flame is similar for both pressures. Interactions between the flame and the flow field can be readily observed. The flame is not uniformly affected by the turbulence; some parts of the flame are being stretched with more intensity than others. An extinction event can be seen in Fig. 9, occurring between 0.3 ms and 0.55 ms, in the lower left quadrant of the computational domain, near x = −0.4 cm and y = 0.5 cm. An dash-dot ellipse in the figure indicates the location of the extinction. The extinguished flame reignites afterward. While the flame is

subjected to similar strain rate at 10 atm, Fig. 10 does not show any discontinuity in the temperature field. This reflects the absence of extinction at higher pressure. Also, more extinction events are observed at 0.1 atm than at 1.0 atm. Using the AEA-based Damköhler number extinction criterion (presented in more details below in Section 4.1), about 7 extinction events are predicted at 0.1 atm, while only 2 are predicted at 1 atm, and none at 10 atm.

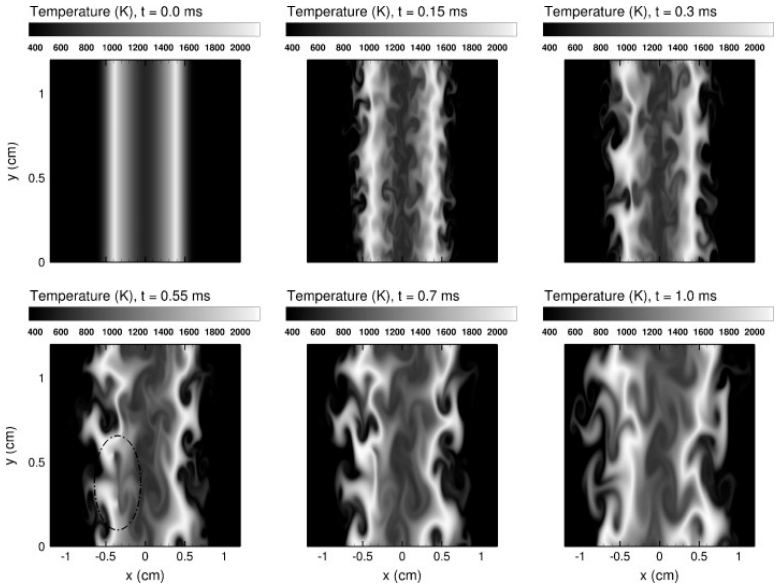

Fig. 9. Instantaneous temperature fields predicted at 1 atm. The progressive wrinkling of the flame is observable as time elapses. Notice the extinction event at 0.55 ms made visible as a region of lower temperatures, as indicated by the dash-dot ellipse.

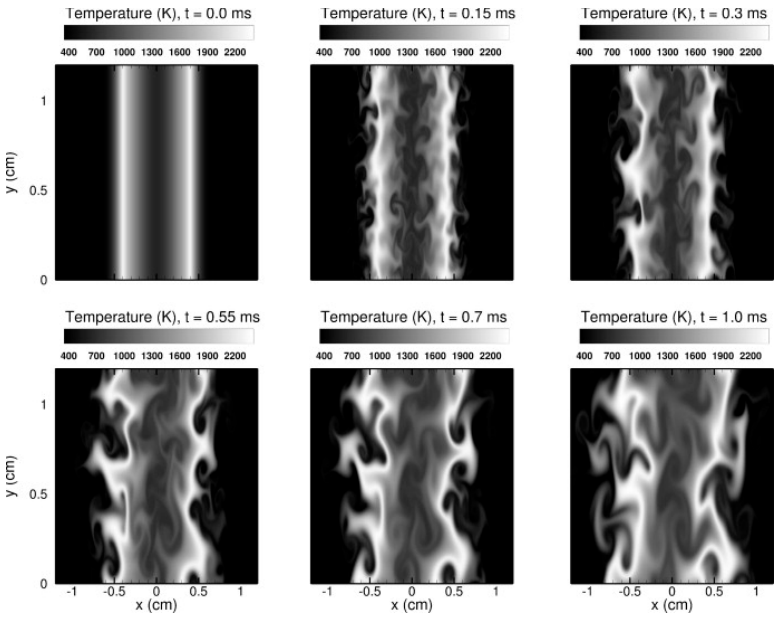

Fig. 10. Instantaneous temperature fields predicted at 10 atm. The progressive wrinkling of the flame is observable as time elapses. Unlike the case at 1 atm, no extinction is predicted.

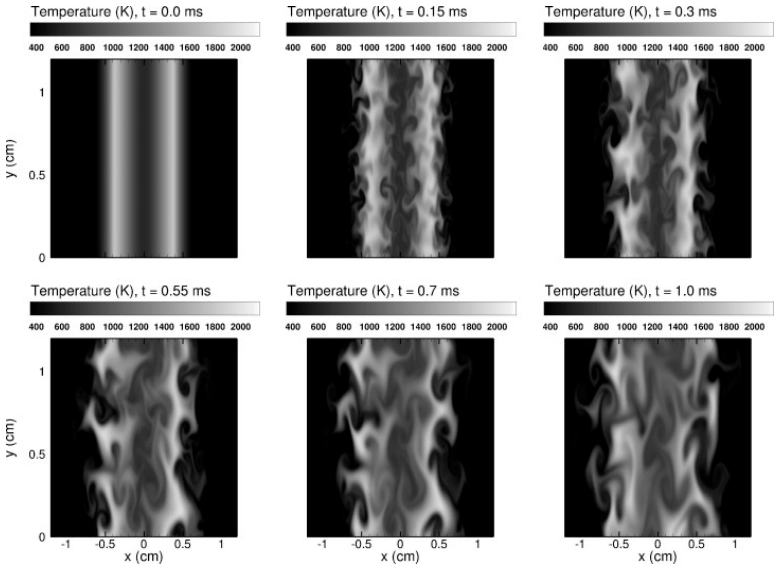

Fig. 11. Instantaneous temperature fields predicted at 0.1 atm. The progressive wrinkling of the flame is observable as time elapses. Several extinction events are predicted.

While the effects of pressure on the turbulence dynamics have been eliminated by manipulating the flow viscosity, pressure effects on the chemistry are still present, as indicated by Fig. 12. Figure 12 plots the temporal evolution of the volume integrated heat release rate for the three pressures considered. A factor of about 10 exists between the three curves and as expected, the heat release rate increases with pressure; more precisely, Fig. 12 suggests that the heat release rate scales linearly with pressure.

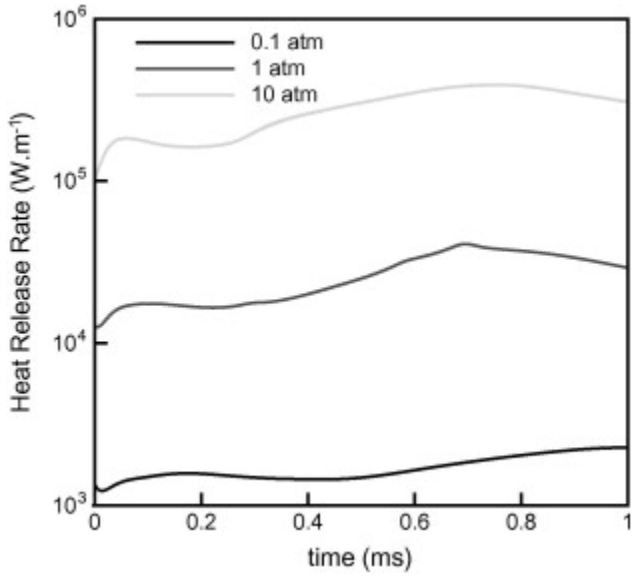

Fig. 12. Temporal evolution of the volume-integrated heat release rate for the three pressure cases considered.

The effects of flow turbulence on the flame are characterized by the value of scalar dissipation rate on the stoichiometric line, χ_{st}. Figure 13 plots the conditional mean of the scalar dissipation rate χ_{st} and its standard deviation for the three pressures. All cases have similar evolution. Starting from an initial value of about 7 s^{-1}, the mean χst quickly reaches a plateau at values near 15 s^{-1}, and remains nearly constant for the first 0.2 ms of the simulation before undergoing a rapid increase, and peaking at approximately 0.4 ms. A slow decrease is observed past the peak. This slow decrease is related to the decrease of the TKE presented in Fig. 8, which

reflects the turbulence decay in this configuration where production mechanisms of turbulence are not present. The standard deviation of χ_{st} follows a similar trend, peaking at the same time as the peak of mean χ_{st}. The predicted standard deviation of χ_{st} is generally greater than the mean value of χ_{st}. This indicates large variations of local flame stretch, and the potential for extinction events. It is important to note that the exact shape of the curves in Fig. 13 depends on the turbulent initial conditions. It is interesting to note that during the later stage of the simulations values of χ_{st} are slightly different, with higher χ_{st} values at lower pressure. This is interpreted as the effect of pressure and temperature on the mixing: the stoichiometric temperature increases with pressure.

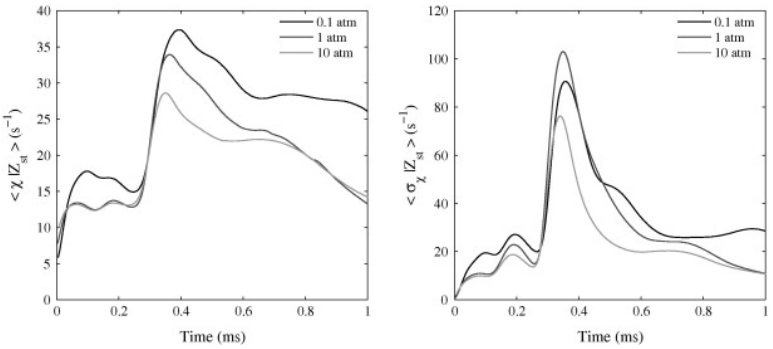

Fig. 13. Temporal evolution of the conditional mean (left) and standard deviation (right) of the stoichiometric scalar dissipation rate at $Z = Z_{st}$ for the three pressure cases considered: 0.1, 1, and 10 atm.

3.3. Effects of the modified viscosity approach on flame properties

Flame extinction characteristics are needed to apply the AEA-based-Damköhler flame extinction diagnostic presented below in Section 4.1. These are namely the stoichiometric scalar dissipation rate, denoted $\chi_{q,ref}$, and the stoichiometric flame temperature, $T_{q,ref}$. Table 1 tabulates these two quantities. These quantities have been obtained from OPPDIF simulations of steady state counter-flow diffusion flames near strain-induced extinction using the aforementioned detailed chemistry model and the modified viscosity approach. $T_{q,ref}$ and $\chi_{q,ref}$ have been calculated for each pressure of interest. At low pressure (P = 0.1 atm), $\chi_{q,ref}$ is 12.5 s^{-1}. $\chi_{q,ref}$ is 95.5 s^{-1} at atmospheric pressure and increases to 465 s^{-1} at 10 atm.

4. Discussion

4.1. AEA-based flame extinction criterion

It is known that for diffusion flames large values of the local flame stretch can lead to aerodynamic quenching [35], [1], [6]. In turbulent diffusion flames, a useful indication of the local flame stretch is given by the scalar dissipation rate at stoichiometry. The scalar dissipation rate may be interpreted as the inverse of a characteristic transport time. In laminar flame theory, this characteristic transport time is compared to a characteristic chemical time through a Damköhler number. In brief, sub-critical burning conditions are observed in diffusion flames when chemistry is fast, i.e. when the characteristic times associated with transport phenomena are larger than the characteristic times associated with chemistry. Similarly, super-critical extinction conditions are observed in diffusion flames when chemistry is slow, i.e. when the characteristic times associated with transport phenomena are shorter than the characteristic times associated with chemistry.

Previous works on extinction limits of laminar counter-flow diffusion flames using DNS [15], [16] and AEA [18], [19] have illustrated the pertinence of a Damköhler-number based flame extinction criterion. In these studies, the transport times scale like $(1/\chi_{st})$ and the chemical times scale like $\exp(T_a/T_{st})$, where T_a is

an activation temperature (a quantity that gives a measure of the sensitivity of the combustion chemistry to changes in temperature) and T_{st} is the flame temperature. One can write the Damköhler number as:

$$(6)\quad Da_{AEA} = C\frac{(1/\chi_{st})}{\exp(T_a/T_{st})} = C\frac{\exp(-T_a/T_{st})}{\chi_{st}},$$

where *C* is a weak function of several flame parameters and is treated here as a constant.
Since Da_{AEA} is dimensionless, *C* has the dimension of inverse time. The AEA analysis of Refs. [18], [19] considers laminar flame extinction due to stretch, cooling, and reactant dilution, and shows that all extinction events correspond to low values of Da_{AEA} and that extinction occurs for a critical value $Da_{AEA,c} \simeq 1$. The parameter *C* in Eq. (6) can therefore be obtained from the knowledge of flame stretch and flame temperature under reference extinction conditions identified by the subscript q,ref:

$$(7)\quad C = \chi_{q,ref}\exp\left(\frac{T_a}{T_{q,ref}}\right).$$

Equation (6) can then be rewritten as:

$$(8)\quad Da_{AEA} = \frac{\chi_{q,ref}}{\chi_{st}}\exp\left(T_a\left(\frac{1}{T_{q,ref}} - \frac{1}{T_{st}}\right)\right).$$

Reference extinction conditions were obtained for the three pressures considered by performing OPPDIF simulations of a counter-flow laminar diffusion flame near its extinction limit [33]. The laminar flame simulations used the same detailed chemistry model as that used in the DNS. The modified viscosity approach was also applied. Table 1tabulates the values of $\chi_{q,ref}$,$T_{q,ref}$, and T_a for the different pressures considered. We present in the next section the approach used to calculate the activation temperature T_a.

4.2. The activation temperature used in the definition of Da_{AEA}

The definition of the AEA-based Damköhler number Da_{AEA} uses an activation temperature, T_a, that provides a measure of the sensitivity of the combustion chemistry to changes in temperatures. Values of T_a were obtained following the methodology presented by Sun et al. [36].

The overall activation energy was determined from a series of laminar premixed flame calculations corresponding to stoichiometric ethylene-oxygen–nitrogen mixtures with different levels of nitrogen dilution. The laminar mass burning rate, $f°$, of a premixed flame is a function of the adiabatic flame temperature, T_{ad}, and activation temperature, T_a, through:

$$(9)\quad f° \sim \exp(-T_a/2T_{ad}).$$

Following Sun et al. [36], T_{ad} can be extracted by calculating the logarithmic derivative of $f°$ with respect to the inverse of T_{ad}:

$$(10)\quad T_a = -2\frac{\partial \ln(f°)}{\partial(1/T_{ad})}.$$

The laminar mass burning rate, $f°$, and the associated adiabatic flame temperature, T_{ad}, were computed for a freely propagating adiabatic flame using PREMIX from the CHEMKIN package [25]. The nitrogen mole fraction was varied from $X_{N_2} = 0.729$ to 0.745. Figure 14 illustrates the change in the temperature profile across the flame when changing the level of nitrogen dilution at 1 atm. Values of T_a were calculated using Eq. (10) at the pressures sought. They are reported in Table 1. Note that all the calculations were performed with PREMIX using the modified viscosity and species diffusion approach presented in Section 2.4.

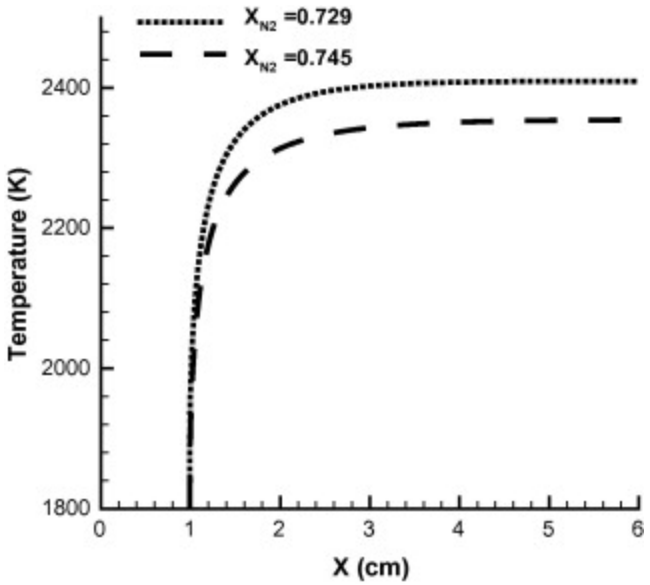

Fig. 14. Temperature profiles of freely propagating, adiabatic stoichiometric ethylene/oxygen premixed flames, with different levels of nitrogen dilution. Pressure is set at 1 atm. Simulations were performed using PREMIX.

In order to illustrate the performance of the extinction diagnostic on flames that departs from the reference case used for calibration, i.e. flame with pure fuel in the fuel stream and air in the oxidizer stream, several extinction limits of diluted ethylene-nitrogen/oxygen–nitrogen laminar counterflow diffusion flames were calculated using OPPDIF [33]at 1 atm. Extinction limits were reached by first calculating a steady state flame far from extinction and then using the previous converged solution as initial solution for the same case but with increased reactants velocity, i.e. increased strain rate. The extinction characteristics were taken from the last converged burning solution for which an increase of reactant stream velocity by no more than 5% leads to a non-burning solution. The fuel stream was a mixture of ethylene and nitrogen. Figure 15 plots the results of these simulations. Flames with diluted fuel stream were sorted in three batches. The first batch corresponds to flames with diluted fuel burning into air. A decrease of fuel mass fraction leads to an increase of the value of stoichiometric mixture fraction Z_{st}. These flames are plotted with circle symbols. The second batch of flames was obtained by holding constant the adiabatic flame temperature T_{ad} and diluting the fuel and the oxidizer stream accordingly. Triangle symbols are used for this batch. The third batch of simulated flames was generated holding constant the flame stoichiometric mixture fraction Z_{st} and diluting the fuel stream and oxidizer stream accordingly. The data are plotted using square symbols. A maximum of fuel dilution of 50% was considered. The case corresponding to pure fuel reacting in air is taken as reference for the three data batches.

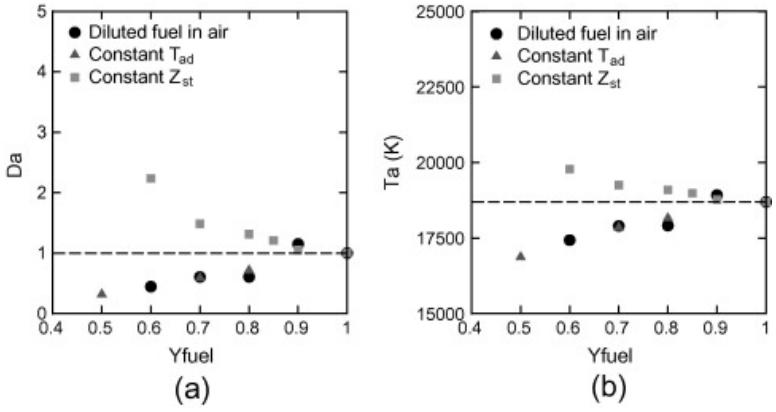

Fig. 15. Calculated *Da* (a) and effective activation temperature *Ta* (b), at the high strain rate extinction limit of laminar counterflow diffusion flameswith different levels of fuel and oxygen dilution plotted against the mass fraction of fuel from the fuel stream. The pressure is set at 1 atm. *Da* near extinction is calculated using Table 1 values. *Ta* near extinction is calculated assuming *Da* = 1 for a given extinction realization.

Figure 15a plots the calculated Da_{AEA} for these flames using the values of Table 1. It is found that in this particular series of test calculations, Da_{AEA} takes values between 0.3 and 2.2. These results suggest that the extinction criterion presented in Eq. (8) is approximate and that deviations of Da_{AEA} by an order of magnitude may be expected. This approximate criterion is still valuable because as shown below, the flame Damköhler number during an extinction event varies by several orders of magnitude.

The same data can be used to calculate an effective global activation temperature T_a for each individual case. Using the same constant C as that of the reference flame and assuming the equality Da_{AEA} = 1 at extinction, then from Eq. (6), T_a can be calculated from the extinction data. Figure 15b plots the value of T_a obtained. Similar behavior to that of Fig. 15a is observed.

It is found that in this particular series of test calculations, the apparent activation temperature T_a takes values between 16,870 K and 19,780 K. These variations are moderate and suggest that the method to evaluate T_a presented in Eq. (10) is suitable.

4.3. DNS evolution of the AEA-based flame extinction criterion

Values of Da_{AEA} have been calculated using Eq. (8) for the three pressure cases. Figure 16 plots selected instantaneous snapshots of the spatial variations of Da_{AEA} along the isocontour of stoichiometric mixture fraction $Z = Z_{st}$, for *P* = 1 atm. Large values of Da_{AEA} correspond to near-equilibrium chemistry and are referred to here as sub-critical conditions, while values of Da_{AEA} below 1 correspond to conditions at or beyond extinction and are referred to here as super-critical conditions. The flame weakest points are defined as local minimum values of Da_{AEA}. Extinction events are defined as locations where $Da_{AEA} < 1$. Figure 16 shows the dynamics of an extinction event that starts at 0.25 ms and lasts until approximately 0.7 ms. This event features extremely low values of Da_{AEA} at 0.305 ms and 0.405 ms. These low values are the result of high gradients and intense mixing conditions. This extinction event is shown in Fig. 9.

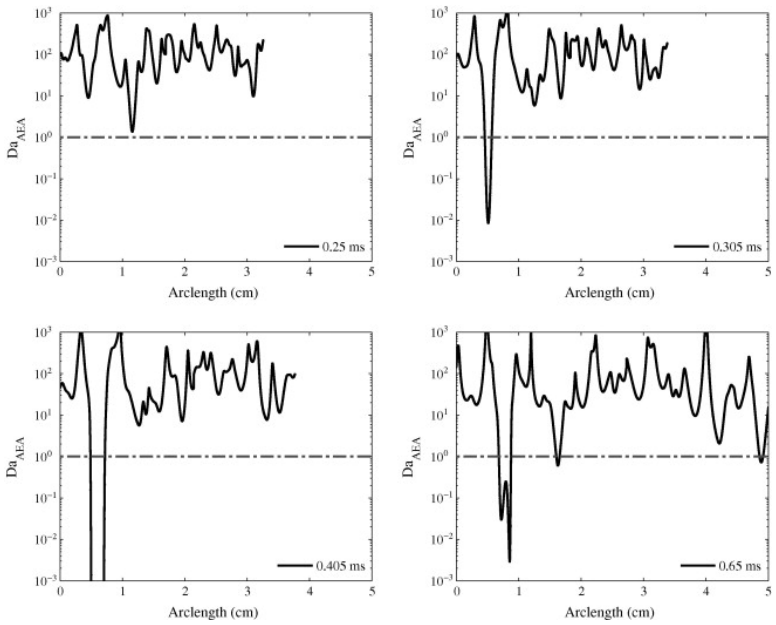

Fig. 16. Spatial variations of the Damköhler number defined by Eq. (8)along the stoichiometric line at 0.25 ms, 0.305 ms, 0.405 ms, and 0.65 ms. Extinction is observed for local conditions where $Da_{AEA} < 1$. An ongoing extinction event takes place between 0.25 ms and 0.65 ms at arclength between 0 and 1 cm. Pressure is 1 atm. The dash-dotted line indicates Da_{AEA} = 1.

The difference in flame extinction behavior when changing pressure is illustrated in Fig. 17. This plot presents the temporal evolution of the conditional mean Damköhler number computed using Eq. (8) and its associated coefficient of variation, defined as the ratio of the standard deviation with the mean, for the three pressures considered. The statistics are calculated along the stoichiometric isocontour. Figure 17shows that high pressure is associated with high values of Da_{AEA}, which indicates a globally stronger flame than that at 0.1 atm. It is interesting to note that there exists a factor of about 10 between each curve, thereby suggesting that Da_{AEA} varies linearly with pressure. The coefficient of variation shows that during most of the simulation the standard deviation of Da_{AEA} is of the same order as the mean Da_{AEA}, which indicates the propensity for local extinction events. In the early stage of the simulation (0–0.3 ms), the coefficient of variation at 0.1 atm is greater than one and bounds the coefficient of variation of Da_{AEA} at 1 and 10 atm.

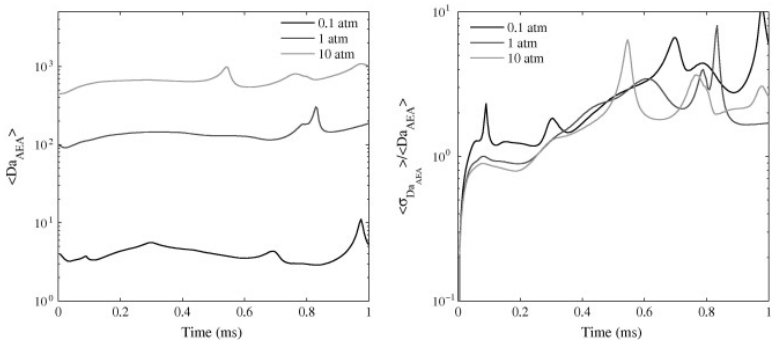

Fig. 17. Temporal evolution of Damköhler number conditional means and their coefficient of variation (standard deviation divided by the mean) for the three pressures considered: 0.1, 1, 10 atm. The Damköhler number has been calculated using Eq. (8) and has been averaged along the stoichiometric isocontour.

In order to push the analysis further, the variation of the local flame structure with varying Da_{AEA} has been analyzed. First we introduce our flame-based diagnostic. The vector $\vec{n} = \nabla Z\,|_{st}/\|\nabla Z\,|_{st}\|$ defines a local unit vector normal to the stoichiometric isocontour. At each location along the flame contour, the DNS solution is explored along the $\vec{n}$ direction and the peak value of selected radical species is recorded. Figure 18 illustrates our methodology. The size of the investigation window was set to 1 mm. This distance was shortened in case of non-monotonous mixture fraction variations to avoid merging effects due to the proximity of other flame fronts.

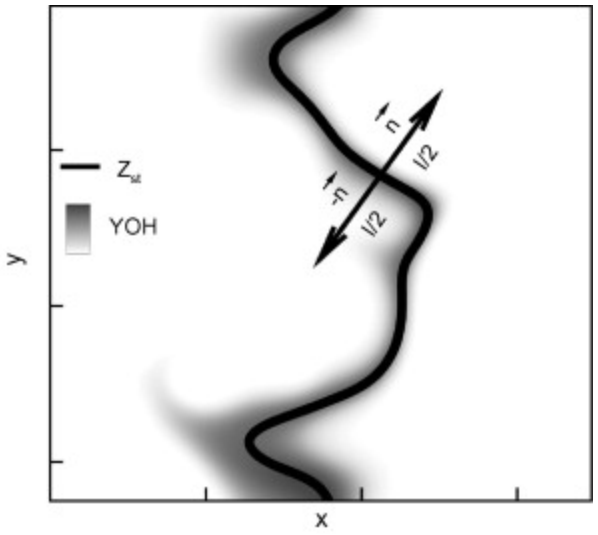

Fig. 18. Methodology to find the local peak value of radicals (OH, H, O, etc.) along the flame surface contour. The solid black line indicates the location of stoichiometry, the gray area represents locations of substantial OH. Maximum values of selected radicals are sought along the direction $\vec{n}$ normal to the line of stoichiometry. The distance of investigation is *l*(typically less than 1 mm) and both fuel and oxidizer sides are considered.

In the following, the local peak value of the radicals OH, H, and O is used to characterize the combustion intensity while the Damköhler number Da_{AEA} (measured on the stoichiometric contour) is used to identify the flame weakest points and the presence of extinction events. Figure 19 presents our post-processing methodology and shows how the flame weakest points are tracked in time. At a time t_i, the Damköhler number Da_{AEA} is calculated on the flame contour, identified as the location of stoichiometric condition. The local minima of Da_{AEA} are interpreted as the flame weakest points. Peak values of radicals OH (noted $Y_{OH,peak}$), H, and O at the flame weakest points are identified using the methodology illustrated in Fig. 18. Finally the values of (Da_{AEA},$Y_{OH,peak}$) are plotted together. The process is then repeated.

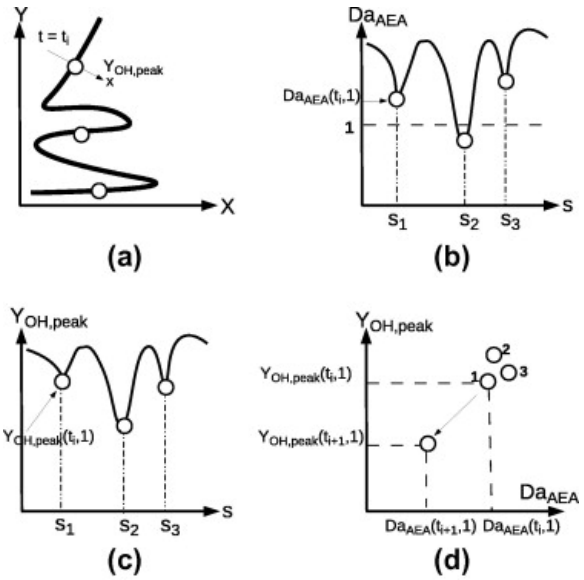

Fig. 19. Sketch representing the analysis of the flame weakest points. First, at a given time ti, the Damköhler number Da_{AEA} is calculated on the flame contour $Z = Z_{st}$ (a). The local minima of Da_{AEA} are interpreted as the flame weakest points (b). The methodology presented in Fig. 18 is then applied to identify the peak values of

radicals OH (noted $Y_{\mathrm{OH},peak}$), H and O at the flame weakest points (c). The values of $Y_{\mathrm{OH},peak}$ and Da_{AEA} at the flame weakest points are then plotted together and the process is repeated at subsequent times (d).

In Fig. 19(d), Da Da_{AEA}AEA provides a measure of the strength of flame elements while peak values of radical mass fraction provide a measure of their chemical activity. Whether these quantities are well correlated provides a simple test to evaluate the validity of the AEA-based Damköhler number concept for flame extinction predictions.

Figure 20 plots the temporal evolution of the peak values of OH, H, and O mass fraction at the flame weakest points as a function of Da_{AEA}. Figure 20 (d) also shows the reaction rate of the elementary reaction $H_2 + O \rightarrow OH + H$ against the associated Da_{AEA}; value of this reaction activation temperature was taken from Law [35]. Each point corresponds to a single time (as explained in Fig. 19) and values were extracted at 0.1 atm, 1.0 atm, and 10 atm. For the 0.1 atm case, 7 different extinction events were observed; 2 for the 1.0 atm case; and none for the 10 atm. For OH, H, and O, a similar qualitative behavior (with some quantitative deviation), is observed regardless of the pressure considered. All plots show a sharp decrease of radical levels with a decrease in Da_{AEA} between approximately 0.1 and 10. While profiles of H and O present some significant scatter, the profile of OH shows the least sensitivity to a change in pressure.

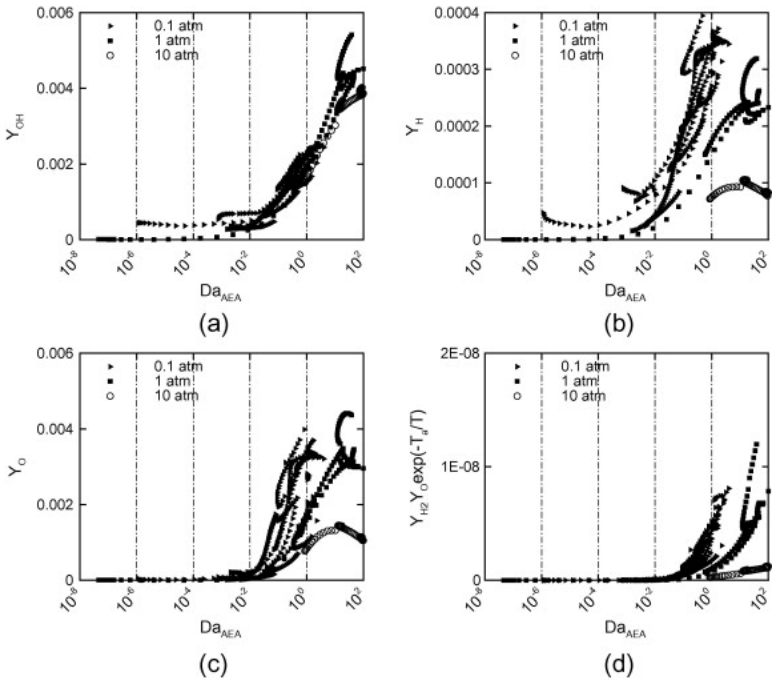

Fig. 20. Analysis of the flame weakening events observed in simulations at 0.1, 1, and 10 atm. Peak value of OH (a), H (b), O (c) mass fraction and $H_2 + O \rightarrow OH + H$ reaction rate (d) as a function of Da_{AEA} at the flame weakest points. This figure has been generated following the methodology presented in Fig. 19.

Among all the radicals presents in this ethylene–air flame, the radical OH is perhaps the most important. Figure 20 shows that regardless of the pressure, a common trend is observed in the evolution of the peak value of Y_{OH} with Da_{AEA}. Three regimes exist. The first regime corresponds to burning conditions observed at large values of Da_{AEA}, typically greater than 10. In this region, a change in Da_{AEA} does not affect significantly the values of Y_{OH}. A transition region exists for Da_{AEA}between 10 and 0.1. In this region, a decrease of Da_{AEA} leads to a strong decrease of Y_{OH}. This is interpreted as the sign of a dramatic weakening of the flame. For values of Da_{AEA} less than 0.1, Y_{OH} decreases by at least one order of magnitude, which is an indication of extinction. A

decrease of OH at the onset of flame extinction has previously been observed in modeling extinction limits of hydrogen spherical diffusion flames using detailed chemistry [37]. This behavior is observed independently of the pressure considered. Note that some non-null values of radicals are observed for some extinction events. This is attributed to the unsteadiness of the flame dynamics. The results presented in Fig. 20suggest that the AEA-based Damköhler number Da_{AEA} which has been derived from asymptotic analysis under the assumption of single step chemistry can be effectively used in detailed chemistry applications and is a valuable metric to identify flame weakening and extinction.

4.4. CEMA-based flame extinction criterion

The Chemical Explosive Mode Analysis (CEMA) has recently been developed and applied to diverse reacting flow configurations: turbulent lifted hydrogen jet flames in hot co-flow [38], turbulent lifted ethylene jet flames [20], perfectly stirred reactors, burner stabilized and free propagating premixed flames, and quasi-homogeneous premixed mixtures of ethylene and n-heptane mixed with air [39]. CEMA is a sophisticated flame diagnostic that provides information on the propensity of a reacting mixture to ignite when a detailed chemical kinetic mechanism is available. CEMA is based on the analysis of the eigenmodes associated with positive eigenvalues of the Jacobian of the chemical source terms.

Considering a reacting system governed by:

$$(11)\ \frac{D\mathbf{y}}{Dt} = \omega(\mathbf{y}) + \mathbf{s}(\mathbf{y}),$$

where ω represents the chemical source terms; $\mathbf{s}$ represents the non-chemical terms; and $\mathbf{y}$ is the state vector of the reactive mixture, for example species concentrations and temperature. A chemical explosive mode (CEM) is an eigenmode of the chemical Jacobian, denoted $\mathbf{J}_\omega$, with its associated eigenvalue that has a positive real part:

$$(12)\ \mathrm{Re}\big(\lambda(\mathbf{J}_\omega)\big) > 0.$$

The zero-crossing of the real part of the CEM has been shown to be correlated with limit flame phenomena, e.g. extinction and ignition, and such flame features as premixed flame fronts [39]. Further details on CEMA are provided in [20], [39] and references therein.

The inverse of the real part of an eigenvalue gives a characteristic time scale associated with a particular chemical mode, $\tau_i = 1/|\ \mathrm{Re}(\lambda_i)\ |$. In CEMA, there is a Damköhler number defined with the CEM timescale and relevant local mixing time. In the present study, the reciprocal scalar dissipation rate at the stoichiometric condition as a characteristic mixing time scale is used to define a new Damköhler number, denoted Da_{CEMA}:

$$(13)\ Da_{CEMA} = -\frac{1/\chi_{st}}{1/\mathrm{Re}(\lambda_e)} = -\frac{\mathrm{Re}(\lambda_e)}{\chi_{st}}.$$

This definition allows for negative and positive values of the Damköhler number. Note that when a CEM is not present, λ_e denotes the eigenvalue of $\mathbf{J}_\omega$ with the largest (least negative) real part. In such cases $Da_{CEMA} > 0$. Otherwise $Da_{CEMA} > 0$. Since the magnitude Da_{CEMA} spans several orders of magnitude, the logarithm of DaCEMA is used as a more convenient way of representation. Since Da_{CEMA} can be negative, its logarithmic expression is modified as:

$$(14)\ \log_{10}(Da_{CEMA}) = -\mathrm{sign}(\mathrm{Re}(\lambda_e))\log_{10}(\max(1, |\ \mathrm{Re}(\lambda_e)\ |/\chi_{st})).$$

This logarithmic representation of Da_{CEMA} is used in the following with a focus on the transition from stable, $\log_{10}(Da_{CEMA}) > 0$, to critical, $Da_{CEMA} = 1, \log_{10}(Da_{CEMA}) = 0$ conditions.

The interpretation of Da_{CEMA} as expressed by Eq. (13) is described below and is further illustrated by Fig. 21. Figure 21 shows the typical S-curve of a PSR configuration showing the state of a chemical reactor as a function of residence time. This curve may also be interpreted as the response of a diffusion flamelet as a function of the inverse of the flame stretch $(1/\chi_{st})$. The upper branch corresponds to the strongly burning regime: when the residence time is very large, the combustion is chemically non-explosive $(\mathrm{Re}(\lambda_e) < 0)$ and $Da_{CEMA} > 0$. When the residence time is reduced, an explosive mode appears beyond which $\mathrm{Re}(\lambda_e) > 0$ and $Da_{CEMA} > 0$. The explosive mode rapidly leads the system to critical conditions where $Da_{CEMA} > 1$ and then to flame extinction. In the logarithmic formulation of Eq. (14), the transition to an explosive mode and the transition to extinction conditions are lumped into a single condition: $\log_{10}(Da_{CEMA}) = 0$.

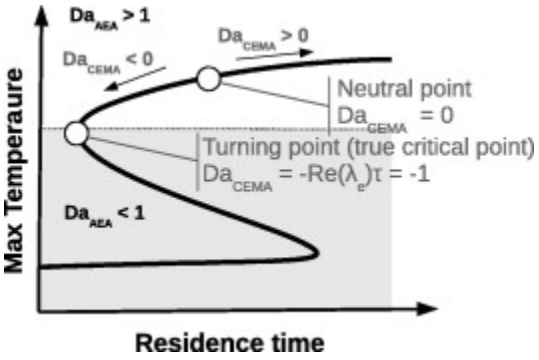

Fig. 21. Schematic illustration of the S-curve obtained in a PSR configuration with location of the different points of transition for the CEMA-based flame extinction criterion. On the upper branch (part non-shaded), two special points are presented. The first one corresponds to $Da_{CEMA} = 0$. This point marks the frontier between a chemically non-explosive ($Da_{CEMA} < 0$) and a chemically explosive ($Da_{CEMA} < 0$) mixture. The second point corresponds to the turning point of the S-curve, which in a PSR configuration corresponds to the location where $Da_{CEMA} = -1$. It corresponds to the point where the timescale of CEM balances that of mixing. Expected values of Da_{AEA} are also indicated in the plot, the shaded part corresponds to $Da_{AEA} < 1$ or super-critical conditions.

CEMA was applied to the 1 atm simulation to extract Da_{CEMA}. Figure 22plots Da_{CEMA} along the stoichiometric isocontour for some selected simulation times: 0.25 ms, 0.30 ms, 0.40 ms, and 0.65 ms. Results show the presence of an explosive mode at several locations along the stoichiometric isocontour. An unstable region is observed between 0.30 ms and past 0.65 ms in the flame segment located between 0 and 1 cm. The size of this unstable region is rather narrow, not exceeding more than 3.5 mm in arclength. Stable conditions are observed along most parts of the stoichiometric isocontour, with Da_{CEMA} greater than 200. In the unstable region, values of Da_{CEMA} can be very low, typically around −1000. This indicates the propensity for local extinction, but still with a characteristic chemical time scale more than two orders of magnitude shorter than the time scale associated with mixing.

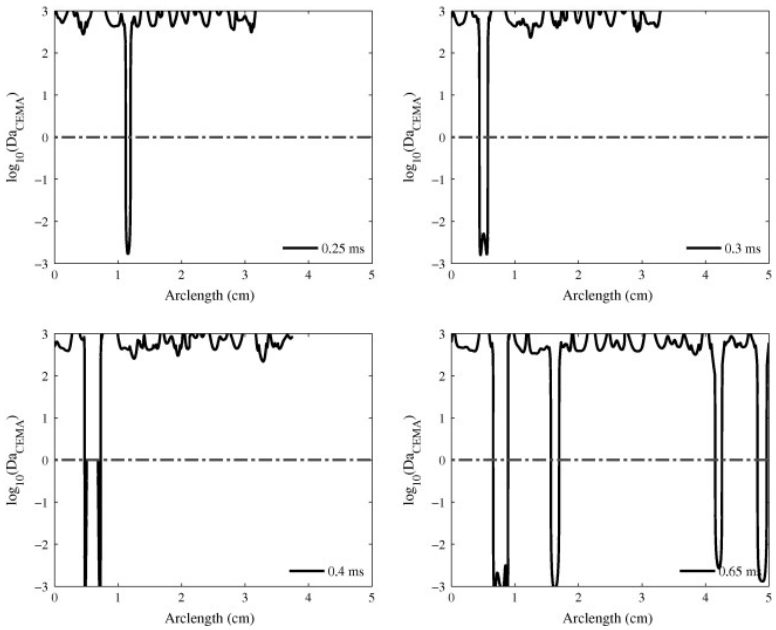

Fig. 22. Spatial variations of $\log_{10}(Da_{CEMA})$ as defined by Eq. (14) along the stoichiometric line at 0.25 ms, 0.305 ms, 0.405 ms, and 0.65 ms. Pressure is 1 atm. The plots are quantitatively similar to those presented in Fig. 16. Values of Da_{CEMA} much larger than unity correspond to stable burning condition; $\log_{10}(Da_{CEMA}) < 0$ correspond to the presence of a chemical explosive mode and transition to extinction.

At 0.40 ms, Fig. 22 shows a well-defined location along the stoichiometric isocontour where $\log_{10}(Da_{CEMA})$ crosses zero. This location of the flame corresponds to transitional critical conditions, i.e. to conditions close to the neutral point and turning point in Fig. 21. We focus in the next section on a comparison between the AEA and CEMA view points for transition to flame extinction.

4.5. Comparison between the AEA-based and CEMA-based Damköhler number

The descriptions of flame extinction have been discussed: AEA and CEMA. The AEA includes a full coupling between the chemistry and transport but is limited to single-step chemistry. It was developed from large activation energy asymptotic analysis in the context of a laminar counter-flow diffusion flame. In contrast, CEMA applies to detailed chemical kinetic systems and to arbitrary combustion configurations but includes only an approximate coupling between chemistry and transport: it is based on an analysis of the Jacobian of the chemistry operator in the combustion equations, not an analysis of the full Jacobian with coupled chemistry and transport. A comparison between AEA and CEMA is presented in this section.

Four flame weak points, corresponding to different parts of the flame contour were identified and tracked (at *P* = 1 atm). The analysis uses the post-processing methodology discussed in Fig. 19. The time evolution of Da_{CEMA} and Da_{AEA} at the flame weak points are reported in Fig. 23(logarithmic scale). The plots present data corresponding to sub-critical conditions ($Da > 1$) and thereby allow a direct comparison of the time at which transition to supercritical conditions (i.e. flame extinction, $Da = 1$) occurs. Note that the AEA theory has questionable meaning beyond extinction, which also explains the limited comparison.

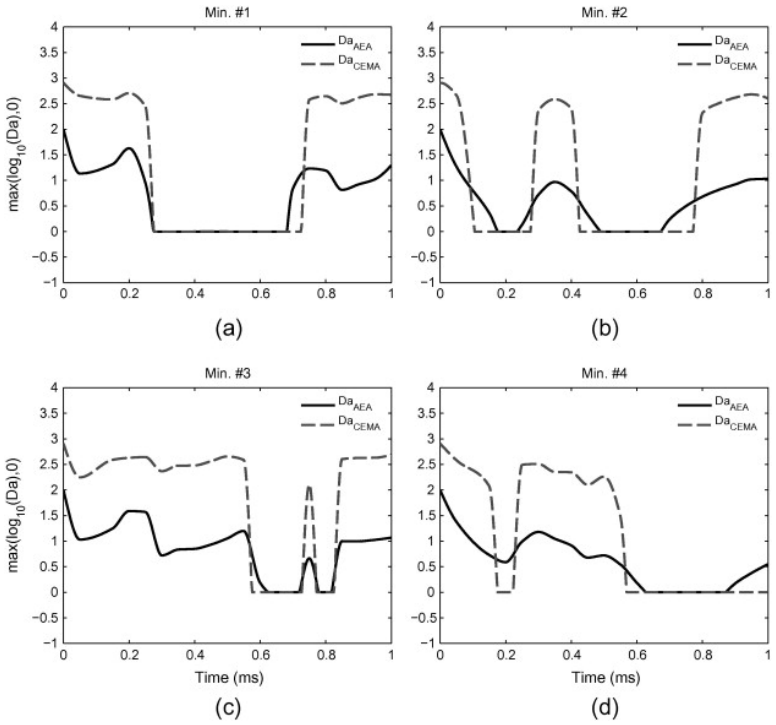

Fig. 23. Temporal evolution of the flame Damköhler number as given by AEA (Da_{AEA}) and CEMA (Da_{CEMA}) at 4 flame weakpoints. Only the portions of the curves corresponding to sub-critical conditions ($Da > 1$) are plotted: this facilitates the identification of the times at which transition to super-critical conditions ($Da = 1$) occurs.

The two diagnostics agree qualitatively well. While the values taken by Da_{AEA} and Da_{CEMA} are significantly different, both quantities are well correlated and predict similar periods of stable burning as well as similar times for flame extinction. The critical times are compared in Fig. 24: this plot contains both critical times corresponding to transitions from sub to super-critical (i.e. extinction) and times corresponding to transition from super to sub-critical (i.e. re-ignition). The agreement between AEA and CEMA is excellent.

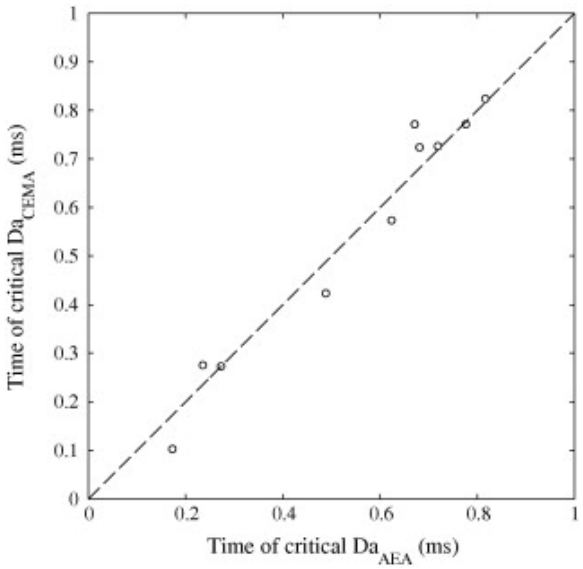

Fig. 24. AEA and CEMA estimates of critical times ($Da = 1$) for the 4 flame weak points analyzed in Fig. 23. The dashed line corresponds a perfect match.

Figure 25 re-plots the complete data set presented in Fig. 23 using a different perspective and provides a direct evaluation of the correlation between Da_{AEA} and Da_{CEMA}. For each segment, the arrows indicate the evolution of time. In each plot, each dot corresponds to a different time realization. The time spacing between each consecutive dots is constant and a large spacing between dots indicates a rapid temporal variation.

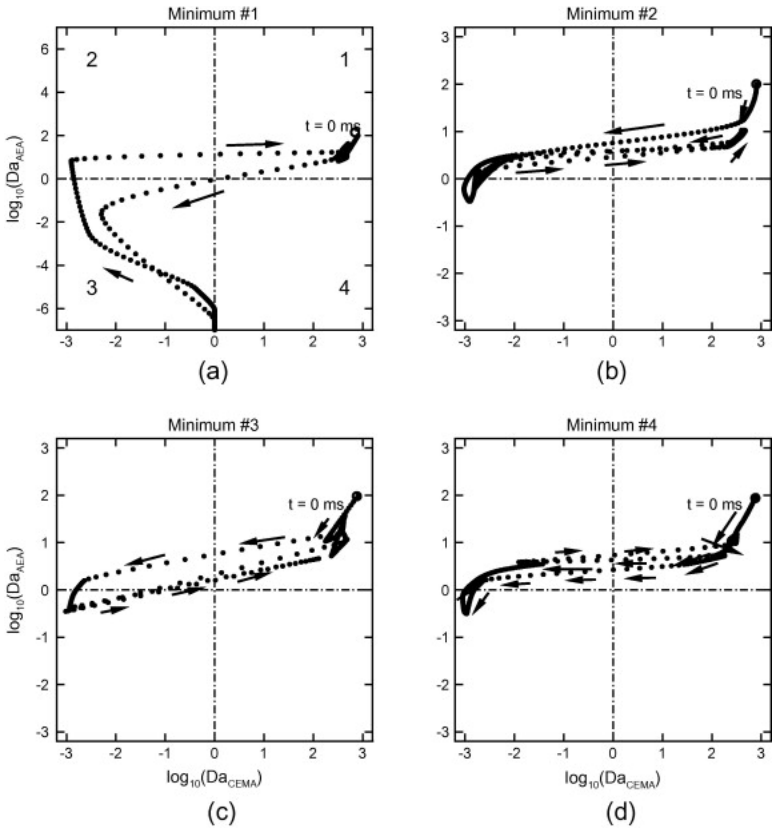

Fig. 25. Discrete temporal trajectories in the phase space (Da_{AEA},Da_{CEMA}) in logarithmic representation for each of the four tracked flame segments presented in Fig. 23. The arrows indicate the time evolution. For each segment, the white dot indicates the value of (Da_{AEA},Da_{CEMA}) at the beginning of the simulation. The phase space (Da_{AEA},Da_{CEMA}) can be divided in four quadrants, depending on the sign of the logarithms. For a given flame segment, each symbol corresponds to a unique time. Time spacing between two consecutive symbols is constant and identical for each segment.

Each (Da_{AEA} and Da_{CEMA}) diagram can be divided into four quadrants centered on (Da_{AEA},Da_{CEMA}) = (1, 1). The upper-right quadrant, denoted 1, corresponds to stable burning conditions. Flame conditions are initially located in this quadrant and will also return to the quadrant after re-ignition.

The upper-left quadrant, denoted 2, corresponds to conflicting AEA and CEMA diagnostics where AEA predicts normal burning while CEMA predicts extinction. This quadrant is occasionally populated in the DNS but the corresponding events are transient between the first and third quadrants.

The lower-left quadrant, denoted 3, corresponds to super-critical conditions. Flame conditions in this quadrant correspond to extinction events. Fairly low spacing between the plotted dots indicates that the trajectories tend to remain in this quadrant for an appreciable amount of time. A notable feature of the flame extinction events is that the transition from stable to unstable conditions appear to be very rapid. This transition occurs for $Da_{AEA} \in [0.1,1]$ and $Da_{CEMA} \in [-1000,100]$.

Finally, the lower-right quadrant, denoted 4, corresponds to conflicting AEA and CEMA diagnostics where AEA predicts extinction while CEMA predicts normal burning. This quadrant remains essentially empty in the DNS.

Overall the level of agreement between the AEA and CEMA Damköler numbers is good and results support the validity of the simplified AEA theory, provided that the activation temperature used in Eq. (8) has been properly calibrated.

5. Conclusion

Direct Numerical Simulations (DNS) of a temporally-evolving ethylene–air diffusion flame immersed in a decaying turbulent flow field were performed for three different cases corresponding to different Damköler number conditions. A modified viscosity and changing pressure (MVCP) scheme was adopted in order to provide isolated control on the flame-flow coupling and the Damköler number conditions. Using MVCP, pressure was changed from the baseline case of 1 atm to 0.1 and 10 atm. In the high pressure MVCP case, the simulated flame is extinction-free, whereas in the low pressure MVCP case, the simulated flame exhibited frequent extinction events and is close to global extinction.

The DNS are first analyzed using large activation energy asymptotic (AEA) theory and a Damköhler-number-based flame extinction criterion. They are also analyzed using Chemical Explosive Mode Analysis (CEMA). AEA includes a full coupling between chemistry and transport but is limited to single-step chemistry and configurations that are similar to laminar counter-flow diffusion flames (i.e. configurations for which the flamelet assumption applies). In contrast, CEMA applies to detailed chemical kinetic systems and to arbitrary combustion configurations but includes only an approximate coupling between chemistry and transport. The comparison between DNS, AEA, and CEMA is very good for transition to extinction events. It is also very good for re-ignition events.

The results show that CEMA can be used to predict critical conditions in turbulent diffusion flames. They also show that AEA can also be used to predict flame extinction, provided that the AEA-based Damköhler number is carefully constructed using a calibrated effective activation temperature.

Acknowledgments

This work was sponsored by the National Science Foundation, PetaApps Program awarded to the multiple institutions, with Grant Nos.: OCI-0904660, OCI-0904480, OCI-0904649, OCI-0904771, OCI-0904818, OCI-0905008. The computational resources for the DNS simulations were supported by the NERSC. The authors would like to acknowledge the contributions of R. Sankaran at Oak Ridge National Laboratory; W. Wang from University of Tennessee; and Kwan-Liu Ma from University of California at Davis, for their help and helpful discussions in this work.

References

[1] A. Liñán Acta Astronaut., 1 (1974), pp. 1007-1039
[2] C.K. Law Combust. Flame, 24 (1975), pp. 89-98
[3] Buckmaster, Lecture 9 spherical diffusion flames, in: Lectures on Mathematical Combustion, vol. 3, 1983, pp. 97–107.
[4] K. Mills, M. Matalon Combust. Sci. Technol., 129 (1997), pp. 295-319
[5] Q. Wang, B.H. Chao Combust. Flame, 158 (2011), pp. 1532-1541
[6] N. Peters Combust. Sci. Technol., 30 (1983), pp. 1-17
[7] F.A. Williams Fire Safety J., 3 (1981), pp. 163-175
[8] F.A. Williams Progr. Energy Combust. Sci., 26 (2000), pp. 657-682

[9] J.C. Hewson, A.R. Kerstein Combust. Sci. Technol., 174 (2002), pp. 35-66
[10] H. Pitsch, C.M. Cha, S. Fedotov Combust. Theory Modell., 7 (2003), pp. 317-332
[11] P. Sripakagorn, S. Mitarai, G. Kosály, H. Pitsch J. Fluid Mech., 518 (2004), pp. 231-259
[12] E.R. Hawkes, R. Sankaran, J.C. Sutherland, J.H. Chen Proc. Combust. Inst., 31 (2007), pp. 1633-1640
[13] R. Venugopal, J. Abraham Combust. Flame, 153 (2008), pp. 442-464
[14] D.O. Lignell, J.H. Chen, H.A. Schmutz Combust. Flame, 158 (2011), pp. 949-963
[15] Y. Wang, A. Trouvé Combust. Flame, 144 (2006), pp. 461-475
[16] P. Narayanan, A. Trouvé Proc. Combust. Inst., 32 (2009), pp. 1481-1489
[17] P.G. Arias, H.G. Im, P. Narayanan, A. Trouvé Proc. Combust. Inst., 33 (2011), pp. 2591-2597
[18] P. Narayanan, H.R. Baum, A. Trouvé Proc. Combust. Inst., 33 (2011), pp. 2539-2546
[19] V. Lecoustre, P. Narayanan, H. Baum, A. Trouve Fire Safety Sci., 10 (2011), pp. 583-595
[20] Z. Luo, C.S. Yoo, E.S. Richardson, J.H. Chen, C.K. Law, T.F. Lu Combust. Flame, 159 (2012), pp. 265-274
[21] C.A. Kennedy, M.H. Carpenter, R.M. Lewis Appl. Numer. Math., 35 (2000), pp. 177-219
[22] C.A. Kennedy, M.H. Carpenter Appl. Numer. Math., 14 (1994), pp. 397-433
[23] M. Baum, T. Poinsot, D. Thévenin J. Comput. Phys., 116 (1995), pp. 247-261
[24] C.S. Yoo, Y. Wang, A. Trouvé, H.G. Im Combust. Theory Modell., 9 (2005), pp. 617-646
[25] R.J. Kee, F.M. Rupley, E. Meeks, J.A. Miller, Chemkin-III: A Fortran Chemical Kinetics Package for the Analysis of Gas-Phase Chemical and Plasma Kinetics, Technical Report May, Sandia National Laboratories, 1996.
[26] J. Appel, H. Bockhorn, M. Frenklach Combust. Flame, 121 (2000), pp. 122-136
[27] T.F. Lu, C.K. Law Progr. Energy Combust. Sci., 35 (2009), pp. 192-215
[28] P.G. Arias, V.R. Lecoustre, S. Roy, W. Wang, Z. Luo, D.C. Haworth, H.G. Im, A. Trouvé, Direct numerical simulation of soot formation and oxidation in temporally evolving turbulent luminous non-premixed flames, in: Fall Technical Meeting of the Eastern States Section of the Combustion Institute, University of Connecticut, Storrs, CT, 2011.
[29] S. Roy, P.G. Arias, V.R. Lecoustre, D.C. Haworth, H.G. Im, A. Trouvé Aerosol Sci. Technol. (2014)
[30] P.G. Arias, V.R. Lecoustre, S. Roy, Z. Luo, D. Haworth, T.F. Lu, A. Trouve, Combust. Flame (2014) (in preparation).
[31] T.F. Lu, C.K. Law J. Phys. Chem. A, 110 (2006), pp. 13202-13208
[32] R.W. Bilger Symp. (Int.) Combust., 22 (1989), pp. 475-488
[33] A.E. Lutz, R.J. Kee, J.F. Grcar, F.M. Rupley, OPPDIF: A Fortran Program for Computing Opposed-Flow Diffusion Flames, Technical Report, Sandia National Laboratories, Report SAND96-8243, 1996.
[34] T. Passot, A. Pouquet J. Fluid Mech., 181 (1987), pp. 441-466
[35] C.K. Law **Combustion Physics** Cambridge University Press (2006)
[36] C.J. Sun, C.J. Sung, L. He, C.K. Law Combust. Flame, 118 (1999), pp. 108-128
[37] V.R. Lecoustre, P.B. Sunderland, B.H. Chao, R.L. Axelbaum Proc. Combust. Inst., 34 (2013), pp. 887-894
[38] T.F. Lu, C.S. Yoo, J.H. Chen, C.K. Law J. Fluid Mech., 652 (2010), pp. 45-64
[39] R. Shan, C.S. Yoo, J.H. Chen, T.F. Lu Combust. Flame, 159 (2012), pp. 3119-3127